Int. J. Multiphase Flow Vol. 17, No. 3, pp. 355–376, 1991
Printed in Great Britain.

0301-9322/91 $3.00 + 0.00

THE DEPOSITION OF PARTICLES ON VERTICAL WALLS

S. T. JOHANSEN
Division of Metallurgy, SINTEF, 7034 Trondheim, Norway

(Received 22 February 1989; in revised form 18 November 1990)

Abstract—A theoretical model for particle deposition on vertical walls is proposed. The model shows that the particle deposition massflux depends on the dimensionless particle relaxion time t_P^+, a dimensionless group Ei representing Brownian motion and the dimensionless group Mi representing electrostatical forces, as well as a new dimensionless group gv/u_τ^3 and the tube Reynolds number. The model represents experimental data on particle deposition very well, and shows how variations in gv/u_τ^3 can reproduce variations in deposition rates similar to those reported in the literature. Outside the Brownian diffusion regime the particle deposition is shown to be controlled by a complex interaction between turbulent migration, dispersion and transversal lift forces.

Key Words: particle deposition, turbulence

INTRODUCTION

The deposition of particles or droplets from turbulent gas flows has been studied extensively during the last 20 years. The understanding and prediction of the deposition massflux is of great interest in areas like pollution control, gas cleaning, design of industrial reactors or transport of particles or droplets in two-phase flow systems. Due to the great interest in the subject, several hundred articles and papers have been published. The deposition of particles on vertical walls is believed to be caused by Brownian diffusion and a turbulent inertial deposition. The Brownian deposition is only of importance for very small (submicron) particles. When the particles become larger, their Brownian diffusivity becomes smaller, but their inertia will result in an increased relative velocity between particles and the turbulent fluctuations of the gas.

The increased relative velocity resulting from increased particle inertia is then believed to be the mechanism which drives the heavy particles through the quiet "laminar sublayer" which is located extremely close to the wall.

The literature on the subject has been reviewed by Papavergos & Hedley (1984). According to their review the scatter in experimental data is extreme, and the maximum deposition rates are between 1 and 3 orders of magnitude larger than the minimum deposition rate when dimensionless quantities are employed. One major reason for the large scatter in the data is that the adhesive forces between particles and walls have not been studied and reported. Davies (1983) points out that the surface roughness is another important factor which can enhance the deposition, but unfortunately most experimental works do not report the condition of the surface.

The deposition process has been described theoretically using three different approaches. The approach most commonly applied employs experimental wall laws for the turbulent diffusivity through the boundary layer. The particle diffusivity is set equal to the turbulent diffusivity of momentum, and the concentration equation is solved through the boundary layer. This has been done by Friedlander & Johnstone (1957), Kneen & Strauss (1969), Owen (1960), Beal (1970) and Davies (1966). In order to obtain agreement between theory and experimental data the workers had to adjust their boundary conditions. The best results were obtained when the particle concentration was set to zero at a particle stopping distance from the wall. The stopping distance is given by a product of the particle relaxation time $t_P = (\rho_P d_P^2)/18\mu$ and some characteristic velocity. Here, ρ_P is the particle density, d_P is the particle diameter and μ is the gas viscosity. However, there is no theoretical justification for this choice. Davies (1966) did not follow the stopping distance concept completely, as he accounted for the fact that the turbulent fluctuations normal to the wall are damped as the wall is approached. A small particle must be closer to the

wall than a larger particle if the wall is to be reached in one free flight. Therefore, Davies (1966) correctly introduced an initial velocity, for the particles free flight, which was reduced for reduced particle inertia. Unfortunately, this approach could not reproduce the experimental data.

A second approach was introduced by Liu & Ilori (1974). They introduced an additional artificial turbulent dispersion of particles, so the particle diffusivity was composed of two added terms. The first term was the standard fluid turbulent viscosity, while the new, second term was the turbulent viscosity multiplied by the ratio t_P/τ_L. The Lagrangian timescale τ_L of the turbulent fluctuations was estimated to drop to zero at the wall, while the particle relaxation time t_P is constant. Hence, the new term strongly exceeds the fluid's diffusivity as the wall is approached. This model seemed to reproduce experimental data (Liu & Agarwal 1974) satisfactorily, but the model lacks a stringent physical and mathematical deduction of the additional particle diffusivity.

A third group of models is based on a random walk or a probabilistic description of the particle movement in the boundary layer. Such theories has been presented by Hutchinson & Hewitt (1971) and Reeks & Skyrme (1976). These theories can reproduce some experiments very well, but the models have introduced model specific thickness of the laminar sublayer. The fluid fluctuations which cause the particles to penetrate the laminar sublayer are taken from regions far from the laminar sublayer, and this is a major weakness of these theories.

Cleaver & Yates (1975) developed a theory for particle deposition based on the bursts and ejections of turbulent fluid into the laminar sublayer. They did not account for the finite dispersion in the core flow, but even so they reproduced experimental data acceptably. The model does not assume any artificial boundary conditions and can therefore claim to be fundamentally founded. Papavergos & Hedley (1979) adopted a synthesis of the model of Cleaver & Yates (1975) and Hutchinson & Hewitt (1971), and they obtained good agreement with their experimental data. However, their model suffers from the weakness of the Hutchinson model discussed above.

In a completely different approach, Rouhiainen & Stachiewicz (1970) investigated the effect of shear-flow-induced lift forces on particles in a boundary layer. They found that this effect can be of considerable importance, although the bulk of the literature on particle deposition has not included this effect in the theoretical analysis. Unfortunately, Rouhiainen & Stachiewicz (1970) did not calculate deposition rates from their theory.

Another effect which influences particle deposition is the turbulent migration. This effect is created by gradients of turbulent energy and imposes a drift velocity on particles in the direction of the solid boundaries. This effect was discussed (probably for the first time) in 1967 by Fortier (1967). He predicted particle deposition from the atmospheric boundary layer and obtained acceptable agreement with the available data. Turbulent migration was the only mechanism he considered. Much later, Reeks (1983) deduced the migration effect from a special closure of the averaged particle Liouville equation. He named the effect "turbophoresis" and showed that turbulent migration could have a strong impact on particle deposition. In a recent paper, Mednikov (1985) stresses the importance of the combination of transversal lift forces and turbulent migration. These effects seem to be of great importance in a theoretical description of sediment transport, but, to date, have not been included in models of particle deposition.

In this paper we will study the effects created by transversal lift and the gradients of turbulent r.m.s. velocities. The results will be employed to predict deposition rates on a fully absorbing vertical wall.

THEORY

The particulate phase can either be described in a Lagrangian or a Eulerian frame of reference. A preliminary investigation in Lagrangian coordinates showed severe problems with a numerically created false drift of particles in the direction of the lower turbulence intensities. The Lagrangian approach was therefore abandoned, though there are no principal limitations which make the Lagrangian description impossible. However, in the near-wall region, where the smallest particles are only influenced by Brownian motion, the Eulerian description is preferable due to significant savings in computer time.

The particulate phase as well as the fluid phase is then described in the Eulerian frame of reference. It is assumed that we have a dilute particle phase where there is no coupling between

the particles and the fluid. Hence, both the fluid mean velocity and turbulence characteristics are assumed undisturbed by the particle phase. A criterion for having a dilute suspension with respect to particle to gas momentum and energy coupling is that the particle phase bulk density is negligible compared with the gas phase, i.e. $\epsilon\rho_P \ll (1-\epsilon)\rho_F$; ϵ is the volume fraction of particles and ρ_F is the gas (fluid) density. The criterion says that diluteness is obtained when the bulk density of the particles is much smaller than the gas bulk density. As $\epsilon \ll 1$, the criterion may be simplified to

$$\epsilon \ll \frac{\rho_F}{\rho_P},$$

which is fulfilled for most experiments on particle deposition reported in the literature.

In the following we will consider heavy particles ($\rho_P/\rho_F \gg 1$) which obey Stokes law ($Re_P \ll 1.0$). The transport equations can now be defined by space-averaged fields (Nigmatulin 1979). The Brownian motions have, in general, been disregarded and the averaging control volumes are restricted, so as to be much larger than the particle size. As discussed by Besnard & Harlow (1988), the averaging procedure makes it impossible to deal with length scales which are small compared with the size of the control volume. Hence, only effects which are due to large-scale turbulence (compared with the particle size) can be represented. In a stationary, two-dimensional situation the continuity equation reads:

$$\frac{\partial}{\partial x}(\epsilon u_P) + \frac{\partial}{\partial y}(\epsilon v_P) - \frac{\partial}{\partial x}\left(D\frac{\partial \epsilon}{\partial x}\right) + \frac{\partial}{\partial y}\left(D\frac{\partial \epsilon}{\partial y}\right) = 0. \qquad [1]$$

Here u_P and v_P are the space-averaged particle velocities in the x and y directions, respectively, ϵ is the particle volume fraction for particles in a size class with volume-averaged diameter d_P and D is the Brownian diffusivity of the particles. In [1] the massflux due to Brownian motions has been reintroduced into the equation via an *ad hoc* hypothesis. This *ad hoc* hypothesis assumes that the Brownian massflux is independent of the "non-Brownian" particle velocities u_P and v_P. Let u_P and x be parallel to the flow direction and the wall, and the x direction is vertical. The conservation of axial momentum now gives

$$\frac{\partial}{\partial x}(\epsilon u_P^2) + \frac{\partial}{\partial y}(\epsilon v_P u_P) = \frac{\epsilon}{t_P}(u_F - u_P)\cdot\left(\frac{C_D \cdot Re_P}{24}\right) + \epsilon g_x; \qquad [2]$$

u_F is the space-averaged fluid velocity parallel to the wall, $t_P = (\rho_P d_P^2)18\mu$ is the Stokes relaxation time and g_x is the component of gravitational acceleration in the flow direction. $Re_P = |\mathbf{u}_F - \mathbf{u}_P| d_P/\nu$ is the particle Reynolds number, C_D is the Re_P-dependent drag function provided by Morsi & Alexander (1972) and ν is the kinematic viscosity of the fluid. It should be noted that several terms (Maxey & Riley 1983) have been omitted in [2], such as the pressure term, virtual mass term and the Basset term. However, the restriction $\rho_P \gg \rho_F$ makes our simplification valid (Hjelmfeldt & Mocros 1966). The particle momentum transport normal to the walls is given by

$$\frac{\partial}{\partial x}(\epsilon u_P v_P) + \frac{\partial}{\partial y}(\epsilon v_P^2) = \frac{\epsilon}{t_P}(v_F - v_P)\left(\frac{C_D \cdot Re_P}{24}\right) + \frac{0.171\epsilon\, d_P}{t_P}(u_F - u_P)\sqrt{\frac{\partial}{\partial y}\left|\frac{u_F}{\nu}\right|} + \frac{\epsilon V_E}{t_P}. \qquad [3]$$

Here v_F is the space-averaged fluid velocity normal to the wall. The last two terms in this equation are the Saffman lift force (Saffman 1965) and the electrostatic force due to mirror charging. The particle acceleration due to mirror charging is given by Boothroyd (1971) as

$$\frac{V_E}{t_P} = \frac{q^2}{t_P 12\pi^2 \varepsilon_0 \mu\, d_P y^2}, \qquad [4]$$

where V_E is an electrostatic drift velocity, q is the particle's electrical charge, ε_0 is the electric permittivity of vacuum, μ is the fluid viscosity and y is the distance between the wall and the origin of the particle. If the particle and the wall are made of poorly conducting materials, the electrical permittivity for the wall and particle material must be introduced into [4] (Hesketh 1977). It should be noted that electrostatic effects due to mirror charging can arise if either the walls or the particles are charged.

Equations [1]–[3] are now simplified by assuming negligible axial gradients of the fields compared with the direction normal to the walls ($\partial/\partial x \approx 0$). The fields u_P, v_P, ϵ, u_F and v_F are now

decomposed into ensemble-averaged ($\bar{U}_P$, $\bar{V}_P$, $\bar{\epsilon}$, $\bar{U}_F$ and $\bar{V}_F$) and fluctuating components (primed), and the resulting equations are finally ensemble-averaged. At this point it is important to stress that we have chosen to work with fields which are first space-averaged and then emsemble-averaged. This approach was judged by Besnard & Harlow (1988) to be especially attractive for the kind of flows in question (dilute flows).

Alternatively, the equations could have been averaged using density weighting or Favre-averaging. This approach seems attractive but necessitates an accurate closure for the density-weighted Reynolds stresses in the inner wall boundary layer. However, to the best of our knowledge, such a closure has not been presented so far.

The ensemble-averaging of the simplified continuity equation now gives

$$\frac{\partial}{\partial y}(\bar{\epsilon}\bar{V}_P) + \frac{\partial}{\partial y}\langle \epsilon' v_P' \rangle - \frac{\partial}{\partial y}\left(D\frac{\partial \bar{\epsilon}}{\partial y}\right) = 0. \quad [5]$$

The $\bar{U}_P$-momentum equation gives (triple correlations of primed quantities are neglected and $C_D \cdot Re_P/24 \approx$ const for near Stokes law particles):

$$\frac{\partial}{\partial y}(\bar{\epsilon}\bar{V}_P\bar{U}_P + \bar{\epsilon}\langle v_P' u_P' \rangle + \bar{V}_P\langle \epsilon' u_P' \rangle + \bar{U}_P\langle \epsilon' v_P' \rangle)$$

$$= \frac{\bar{\epsilon}}{t_P}(\bar{U}_F - \bar{U}_P)\cdot\frac{C_D \cdot Re_P}{24} + \frac{\langle \epsilon' u_F' \rangle - \langle \epsilon' u_P' \rangle}{t_P}\cdot\left(\frac{C_D \cdot Re_P}{24}\right) + \bar{\epsilon}g_x. \quad [6]$$

By noticing that the wall massflux is $J\rho_P$, we obtain from [5], for the flux J:

$$J = \bar{\epsilon}\bar{V}_P + \langle \epsilon' v_P' \rangle - D\frac{\partial \bar{\epsilon}}{\partial y}. \quad [7]$$

After [7] is introduced into [6], we obtain

$$\frac{\partial \bar{U}_P}{\partial y} = -\frac{\partial}{\partial y}\left(D\frac{\partial \bar{\epsilon}}{\partial y}\bar{U}_P + \epsilon\langle u_P' v_P' \rangle + \bar{V}\langle \epsilon' u_P' \rangle\right)$$

$$+ \frac{\bar{\epsilon}}{t_P}(\bar{U}_F - \bar{U}_P)\cdot\left(\frac{C_D \cdot Re_P}{24}\right) + \frac{\langle \epsilon' u_F' \rangle - \langle \epsilon' u_P' \rangle}{t_P}\cdot\left(\frac{C_D \cdot Re_P}{24}\right) + \bar{\epsilon}g_x. \quad [8]$$

A similar treatment of [3] for particle momentum normal to the walls yields:

$$(J + \langle \epsilon' v_P' \rangle)\frac{\partial \bar{V}_P}{\partial y} = -\frac{\partial}{\partial y}\left(D\frac{\partial \bar{\epsilon}}{\partial y}\bar{V}_P + \bar{\epsilon}\langle v_P'^2 \rangle\right) - \bar{V}_P\frac{\partial}{\partial y}\langle \epsilon' v_P' \rangle$$

$$+ \frac{\bar{\epsilon}}{t_P}(\bar{V}_F - \bar{V}_P)\cdot\left(\frac{C_D \cdot Re_P}{24}\right) + \frac{(\langle \epsilon' v_F' \rangle - \langle \epsilon' v_P' \rangle)}{t_P}\cdot\left(\frac{C_D \cdot Re_P}{24}\right)$$

$$+ \frac{0.171\, d_P}{t_P}\left(\bar{\epsilon}(\bar{U}_F - \bar{U}_P)\sqrt{\frac{\partial}{\partial y}\left|\frac{\bar{U}_F}{\nu}\right|} + \langle s \rangle\right) - \frac{\bar{\epsilon}V_E}{t_P}. \quad [9]$$

The quantity $\langle s \rangle$ is here defined by

$$\langle s \rangle \equiv \left\langle \epsilon(u_F - u_P)\sqrt{\frac{\partial}{\partial y}\left|\frac{u_F}{\nu}\right|} \right\rangle - \bar{\epsilon}(\bar{U}_F - \bar{U}_P)\sqrt{\frac{\partial}{\partial y}\left|\frac{\bar{U}_F}{\nu}\right|}. \quad [10]$$

The particle transport is now described by [5] and [7]–[9]. However, the equations contain unknown correlations which must be determined in order to close the set of equations.

As we have assumed negligible axial gradients of all fields, the correlation between volume fraction fluctuations (ϵ') and axial velocity fluctuations (u_F', u_P') must disappear. The correlations $\langle \epsilon' v_P' \rangle$ and $\langle \epsilon' v_F' \rangle$ are modelled via gradient diffusion (Pourahmadi 1982):

$$\langle \epsilon' v_P' \rangle = -\nu_t^P\frac{\partial \epsilon}{\partial y}. \quad [11]$$

However, the difference flux $\langle \epsilon' v'_F \rangle - \langle \epsilon' v'_P \rangle$ is assumed to take the isotropic flow value obtained from [9]:

$$(\langle \epsilon' v'_F \rangle - \langle \epsilon' v_P \rangle)\left(\frac{C_D \cdot Re_P}{24}\right) = t_P \langle v'^2_F \rangle \frac{\partial \epsilon}{\partial y}. \quad [12]$$

The long-time particle dispersion coefficient v_t^P has in several works (Gouesbet *et al.* 1984; Desjonquers *et al.* 1986) been predicted to be identical to the fluid diffusivity v_t. However, external fields such as gravity will cause crossing particle and fluid trajectories. Hence, the particle's residence time within a turbulent eddy becomes shorter than the lifetime of the eddy. The result is that the particle dispersion coefficient (v_t^P) will become smaller and smaller, compared with the fluid eddy diffusivity v_t, as the particle settling velocity increases. Picart *et al.* (1986) found that a good estimate for v is

$$v_t^P = \frac{v_t}{\sqrt{1 + \dfrac{0.85|\bar{V}_{P,i} - \bar{V}_{F,i}|^2}{\dfrac{2k_e}{3}}}}, \quad [13a]$$

where $|\bar{V}_{P,i} - \bar{V}_{F,i}|$ is the magnitude of the interphasial relative velocity and k_e is the kinetic energy of the turbulent velocity fluctuations,

$$k_e = \frac{1}{2}\sum_{i=1}^{3} \langle v'^2_{F,i} \rangle.$$

If the particles are very small they may show Schmidt numbers < 1.0. In this case the turbulent dispersion of particles will be overpredicted by [13a] due to an additional coupling between Brownian motions and turbulent dispersion. This can be reflected via a turbulent, Brownian motion induced, Schmidt number Sc_t^*.

Reynolds (1975) predicted v_t^P to be

$$v_t^P = \frac{v_t}{Sc_t^*} = \frac{\langle v'^2_F \rangle \cdot \tau_L}{1 + \dfrac{\tau_L}{\tau_m}}, \quad [13b]$$

where τ_L is the Lagrangian timescale of the fluid and τ_m is the relaxation time for diffusion. The ratio τ_L/τ_m was estimated by Reynolds to be

$$\frac{\tau_L}{\tau_m} = c_1 \cdot \left(\frac{v_t}{D}\right)^{-1/2}. \quad [14]$$

The turbulent diffusivity of the fluid is $v_t = \langle v'^2_F \rangle \cdot \tau_L$ (Rogers *et al.* 1986) and, by taking the constant $c_1 = 1.0$, the Brownian contribution to the turbulent Schmidt number becomes

$$Sc_t^* = 1 + \sqrt{\frac{D}{v_t}}. \quad [15]$$

The final dispersion coefficient for the particles is obtained by combining [13a], [13b] and [15] to obtain

$$v_t^P = \frac{v_t}{Sc_t}, \quad [16a]$$

where the effective turbulent Schmidt number Sc_t is given by

$$Sc_t = \left(1 + \sqrt{\frac{D}{v_t}}\right)\left(1 + \frac{0.85|\bar{V}_{P,i} - \bar{V}_{F,i}|^2}{\dfrac{2k_e}{3}}\right)^{1/2}. \quad [16b]$$

The Brownian contribution to the turbulent Schmidt number causes a reduction in v_t^P in regions where $D > v_t$, and is, at least, in qualitative agreement with experience with heat flow in low Prandtl number fluids (Launder 1978). In regions with large relative velocities and low values of the

turbulent kinetic energy k_e, typical of the inner wall layer, the reduction in ν_t^P due to the "crossing trajectory" effect may be significant.

The ensemble-averaged squared particle fluctuating velocity $\langle v_P'^2 \rangle$ normal to the wall is due to Pourahmadi (1982):

$$\langle v_P'^2 \rangle = \langle v_F'^2 \rangle \left(1 + \frac{t_P}{\tau_L}\right)^{-1}. \quad [17]$$

However, this relation assumes an equilibrium situation where the particles have infinite time to adjust to the fluctuations of the fluid. In particle deposition, where there might be a significant movement of particles through the wall boundary layer, the assumption of equilibrium is somewhat doubtful. Particles which travel through regions with sharp gradients in turbulent r.m.s. velocity will not "feel" the changing background fluid field if the particle relaxation length l_r is larger than the thickness of the region. A crude criterion for equilibrium is

$$l_r = \sqrt{\langle v_P'^2 \rangle} \cdot t_P \ll \delta, \quad [18]$$

where $\sqrt{\langle v_P'^2 \rangle}$ is a typical particle r.m.s. velocity and δ is the thickness of the buffer layer. If wall variables are introduced, [18] can be made dimensionless:

$$\sqrt{\langle v_P'^2 \rangle^+} \cdot t_P^+ \ll \delta^+. \quad [19]$$

Here $\langle v_P'^2 \rangle = \langle v_P'^2 \rangle / u_\tau^2$, $t_P^+ = t_P \cdot u_\tau^2 / \nu$, $\delta^+ = \delta \cdot u_\tau / \nu$ and the wall shear velocity is $u_\tau = \sqrt{\tau_w / \rho_F}$, where τ_w is the wall shear stress. In the literature (Reeks & Skyrme 1976) a typical Lagrangian timescale $\tau_L^+ = \tau_L \cdot u_\tau^2 / \nu$ in the buffer layer is reported to be $\tau_L^+ \approx 11.0$. The maximum value of $\langle v_F'^2 \rangle / u_\tau^2$ is close to 0.64 (Kim *et al.* 1987) at the edge of the buffer layer. The thickness of the buffer layer is typically $\delta^+ \approx 30$. Introduced into [17] and [19] these values give reasonable equilibrium particle r.m.s. velocities for

$$t_P^+ \ll 138. \quad [20]$$

A stringent prediction of the particle r.m.s. velocity for a typical nonequilibrium situation involves the solution of transport equations for the particle r.m.s. velocities. This approach offers several theoretical complications which are avoided in the present work. As we will see below, the accurate representation of particle r.m.s. velocities plays only a limited role in the deposition of larger particles ($t_P^+ > 10$). We have therefore employed the equilibrium condition given by [17], as a first approach.

According to Pourahmadi (1982) the correlation $\langle u_P' v_P' \rangle$ is modelled as

$$\langle u_P' v_P' \rangle = -\nu_P \frac{\partial \bar{U}_P}{\partial y}. \quad [21]$$

The last term we have to consider is $\langle s \rangle$ from [10]. This is a highly nonlinear term which is difficult to estimate. However, we know that the turbulent transport is directed in the y direction since $\partial / \partial x = 0$. The transport in the y direction is driven by the turbulent fluctuations v_F'. Since v_F' or v_P' do not enter [10] it is plausible to assume that

$$\langle s \rangle = 0. \quad [22]$$

Dimensionless Formulation of the Governing Equations

We can now introduce our modelling correlations into [7]–[9]. At the same time we introduce dimensionless variables into all the equations. From [7] we obtain

$$J^+ = \frac{J}{u_\tau \epsilon_B} = \bar{\epsilon}^+ \bar{V}_P^+ - \left(\frac{\nu_t^+}{Sc_t} + \frac{1}{Sc}\right) \frac{\partial \epsilon^+}{\partial y^+}. \quad [23]$$

Here ϵ_B is the bulk particle volume fraction far from the wall, $\nu_t^+ = \nu_t / \nu$, $y^+ = y \cdot u_\tau / \nu$, Sc_t is given by [16b] and the inverse Schmidt number is, for Brownian motion, represented by the Einstein diffusivity:

$$\mathrm{Sc}^{-1} = \frac{D}{\nu} = \frac{kT}{3\pi\mu d_\mathrm{P}\nu}, \qquad [24]$$

where k is Boltzmann's constant, T is the absolute temperature and μ is the fluid viscosity.

For particles with Knudsen number <1 ($\mathrm{Kn} = d_\mathrm{P}/2\lambda_\mathrm{F}$, λ_F is the gas molecule mean-free-path), the Brownian diffusivity is inaccurately represented by $D = kT/3\pi\mu d_\mathrm{P}$ and must be corrected (Talbot *et al.* 1980). If we introduce the dimensionless particle diameter $d_\mathrm{P}^+ = d_\mathrm{P}u_\tau/\nu$ into [24], we obtain

$$\mathrm{Sc}^{-1} = \frac{kTu_\tau}{3\pi\mu\nu^2 d_\mathrm{P}^+} = \frac{\mathrm{Ei}}{d_\mathrm{P}^+}. \qquad [25]$$

We have now introduced a dimensionless Einstein number Ei in order to make all quantities and fields dimensionless. The Einstein number is given by

$$\mathrm{Ei} = \frac{kTu_\tau}{3\pi\mu\nu^2}. \qquad [26]$$

The modelled and dimensionless form of [8] is now

$$J^+\frac{\partial \bar{U}_\mathrm{P}^+}{\partial y^+} = -\frac{\partial}{\partial y^+}\left(\mathrm{Sc}^{-1}\frac{\partial \bar{\epsilon}^+}{\partial y^+} - \bar{\epsilon}^+ v_\mathrm{P}^+\frac{\partial \bar{U}_\mathrm{P}^+}{\partial y^+}\right) + \frac{\bar{\epsilon}^+}{t_\mathrm{P}^+}(\bar{U}_\mathrm{F}^+ - \bar{U}_\mathrm{P}^+)\cdot\left(\frac{C_\mathrm{D}\,\mathrm{Re}_\mathrm{P}}{24}\right) - \bar{\epsilon}^+\left(\frac{g_x\nu}{u_\tau^3}\right), \qquad [27]$$

where the dimensionless particle relaxation time is given by

$$t_\mathrm{P}^+ = t_\mathrm{P}\cdot\frac{u_\tau^2}{\nu}. \qquad [28]$$

Similarly, we obtain from [9] and our modelling assumptions ($\bar{V}_\mathrm{F}^+ = 0$):

$$\begin{aligned}\left(J^+ - v_\mathrm{P}^+\frac{\partial \bar{\epsilon}^+}{\partial y^+}\right)\frac{\partial \bar{V}_\mathrm{P}^+}{\partial y^+} = {} & -\frac{\partial}{\partial y^+}\left(\mathrm{Sc}^{-1}\frac{\partial \bar{\epsilon}^+}{\partial y^+}\bar{V}_\mathrm{P}^+\right) - \bar{\epsilon}^+\frac{\partial}{\partial y^+}\langle v_\mathrm{P}'^2\rangle^+ \\ & + \bar{V}_\mathrm{P}^+\frac{\partial}{\partial y^+}\left(v_\mathrm{P}^+\frac{\partial \bar{\epsilon}^+}{\partial y^+}\right) - \frac{\bar{\epsilon}^+\bar{V}_\mathrm{P}^+}{t_\mathrm{P}^+}\cdot\left(\frac{C_\mathrm{D}\cdot\mathrm{Re}_\mathrm{P}}{24}\right) \\ & + \frac{0.171 d^+}{t_\mathrm{P}^+}\bar{\epsilon}^+(\bar{U}_\mathrm{F}^+ - \bar{U}_\mathrm{P}^+)\sqrt{\frac{\partial}{\partial y^+}|\bar{U}_\mathrm{F}^+|} - \frac{\bar{\epsilon}^+ V_\mathrm{E}^+}{t_\mathrm{P}^+}. \end{aligned} \qquad [29]$$

The dimensionless "drift velocity" V_E^+, taken from [4] is now written as

$$V_\mathrm{E}^+ = \frac{\mathrm{Mi}}{d^+ y^{+2}}, \qquad [30]$$

where the dimensionless group Mi representing mirror charging is

$$\mathrm{Mi} = \frac{q^2 u_\tau^3}{12\pi^2\varepsilon_0\mu\nu^3}. \qquad [31]$$

To complete the model we need a good representation of the turbulent kinematic viscosity ν_t^+, the Lagrangian timescale τ_L^+, the fluid r.m.s. velocity $\langle v_\mathrm{F}'^2\rangle$ and the mean fluid velocity $\bar{U}_\mathrm{F}$ throughout the boundary layer. However, ν_t^+ is given as

$$\nu_\mathrm{t}^+ = \langle v_\mathrm{F}'^2\rangle^+\tau_\mathrm{L}^+ \qquad [32]$$

and the velocity profile in a one-dimensional boundary layer with negligible pressure gradient is (Tennekes & Lumley 1972):

$$\bar{U}_\mathrm{F}^+(y^+) = \int_0^{y^+}\frac{\mathrm{d}y^+}{1+\nu_\mathrm{t}^+}. \qquad [33]$$

Hence, we only need a good and, if possible, general representation of ν_t^+ and $\langle v_\mathrm{F}'^2\rangle^+$.

We have chosen ν_t^+ to be:

$$\nu_t^+ = \begin{cases} \left(\frac{y^+}{11.15}\right)^3, & y^+ < 3.0, \\ \left(\frac{y^+}{11.4}\right)^2 - 0.049774, & y^+ \in [3.0, 52.108], \\ 0.4y^+, & y^+ > 52.108. \end{cases} \quad [34]$$

The value of ν_t^+ for $y^+ \to 0$ is in accord with the direct simulation of turbulence in a channel by Kim *et al.* (1987). The velocity profile obtained from [33] and [34] is in very good agreement with Kim *et al.*'s simulated velocity profile (Johansen & Ytrehus 1988).

A representation of the fluid normal r.m.s. velocity is chosen in accord with the results from Kim *et al.* (1987) and the measurements of Kutateladze *et al.* (1979):

$$v'(y^+)^+ = \sqrt{\langle v_F'^2 \rangle^+} = \begin{cases} 0.033\, y^+ \left[1 - \exp\left(-\frac{y^+}{3.837}\right)\right], & \\ \exp\left[\frac{-\left(\frac{y^+}{30.0}\right)^{7.82}}{7.82}\right], & y^+ \leqslant 30.0, \\ v'(30.0)^+ - [v'(30.0)^+ - 0.65]\frac{(y^+ - 30.0)}{(R^+ - 30.0)}, & y^+ \in \langle 30.0, R^+], \end{cases} \quad [35]$$

where R^+ is the dimensionless channel half-width or the dimensionless tube radius. The Lagrangian timescale is now obtained from [32], [34] and [35] by

$$\tau_L^+ = \frac{\nu_t^+}{\langle v_F'^2 \rangle^+}. \quad [36]$$

The velocity profile $\bar{U}_F^+(y^+)$ which results from [33] and [34] is

$$\bar{U}_F^+ = \begin{cases} 11.4 \tan^{-1}\left(\frac{y^+}{11.4}\right) & y^+ \leqslant y_1^+, \\ \bar{U}_F^+(y_1^+) + 2.5 \ln\left(\frac{1 + 0.4y^+}{1 + 0.4y_1^+}\right), & y^+ > y_1^+, \\ \text{where } y_1^+ = 52.984. & \end{cases} \quad [37]$$

The representation of the fluid fields concludes our model, which is given by the [23], [27] and [29]. The dimensionless form of the model simplifies the study of the quantities which play a role in the deposition process. The actual dimensionless quantities are the Einstein number Ei, the mirror charging group Mi, the channel or tube half-width R^+, the gravity group $(g_x \nu / u_\tau^3)$ in [27], the dimensionless particle diameter d_P^+ and the dimensionless particle relaxation time t_P^+. However, d_P^+ is linked to t_P^+ by

$$t_P^+ = \frac{\rho_P d_P^2}{18\mu} \frac{u_\tau^2}{\nu} = \left(\frac{\rho_P}{\rho_F}\right) \frac{d_P^{+2}}{18}. \quad [38]$$

Hence, the density ratio ρ_P/ρ_F, t_P^+, Ei, Mi, R^+ and $(g_x \nu / u_\tau^3)$ are the dimensionless quantities which will describe the deposition flux in the present theory.

Some of the physics contained in [23], [27] and [29] can be investigated by some simple considerations. Let us assume that the particles do not adhere to the wall material and no electrical charges are present, so there is a zero deposition flux ($J^+ = 0$). All the terms with second order

in $\partial/\partial y^+$ are neglected in [27] and [29]. Hence, for Stokes law particles ($C_D = 24/Re_p$) the axial particle velocity becomes

$$\bar{U}_P^+ = \bar{U}_F^+ + t_P^+ \left(\frac{g_x \nu}{u_\tau^3}\right) \qquad [39]$$

and the normal to wall particle velocity component is, with help from [39]:

$$\bar{V}_P^+ = -t_P^+ \frac{\partial}{\partial y^+} \langle v_P'^2 \rangle^+ - 0.171\, d_P^+ t_P^+ \left(\frac{g_x \nu}{u_\tau^3}\right) \sqrt{\frac{\partial}{\partial y^+} |\bar{U}_F^+|}. \qquad [40]$$

The first r.h.s. term in [40] represents the turbulent migration. The turbulent migration term is $t_P^+(\partial/\partial y^+)\langle v_P'^2 \rangle^+$, which is similar to the expression quoted by Mednikov (1985). Since the gradient in $\langle v_P'^2 \rangle^+$ is steep in the buffer layer ($y^+ < 30$, see [35]), the migration term causes a drift of the particles towards the wall.

The last term expresses the drift caused by the transversal lift in a shear flow. When the x-component of gravity is directed in the flow direction the lift force will enhance the transport towards the wall. If the flow direction is reversed the lift force will cause a migration away from the wall.

If we now consider a situation where the gravity vector points in the flow direction we should expect particles to migrate towards the wall. From [23] we obtain:

$$\bar{\epsilon}^+ \bar{V}_P^+ = (\nu_P^+ + \mathrm{Sc}^{-1}) \frac{\partial \epsilon^+}{\partial y^+}. \qquad [41]$$

The particle migration will in this situation, if the particles are not absorbed by the wall, cause a buildup of particles close to the wall. Equilibrium is obtained when the diffusive transport away from the wall balances the migration flux in the opposite direction. The equilibrium concentration is obtained from [41]:

$$\overline{\epsilon^+} = \overline{\epsilon^+}(R^+) \exp\left(-\int_{y^+}^{R^+} \frac{\overline{V_P^+}\, dy^+}{\nu_t^+ + \mathrm{Sc}^{-1}}\right),$$

where $\overline{\epsilon^+}(R^+)$ is the bulk void fraction of particles. A constant and negative $\overline{V_P^+}$ will then cause a buildup in the boundary layer. In the Brownian diffusion boundary layer, the concentration will increase exponentially with reduced y^+ if $\overline{V_P^+} \approx$ const.

APPLICATION OF THE MODEL TO TUBE FLOW

The equations which describe the particle volume fraction and velocities ([23], [27] and [29]) are strongly coupled and cannot be solved by analytical means. We have therefore adopted a numerical procedure, which will be described in this section.

Most data on particle deposition is available for tube flows. Hence, it is natural to verify our model against experimental results for tubes. As the major variations in the particle concentration and the radial particle drift velocity are confined to a small region close to the walls, the governing equations are kept in cartesian notation. The governing equations are mainly first-order ordinary differential equations. Equation [27], which describe U_P-momentum, is, however, second order. We therefore need one boundary condition for $\bar{\epsilon}$ and $\bar{V}_P$ each, while we need two for $\bar{U}_P$. The boundary conditions were taken as:

$$\bar{\epsilon}^+ \left(y^+ = \frac{d_P^+}{2}\right) = 0,$$

$$\bar{V}^+(y^+ = R^+) = 0,$$

$$\bar{U}_P^+(y^+ = R^+) = \bar{U}_F^+(R^+) + t_P^+ \left(\frac{g\nu}{u_\tau^3}\right)\left(\frac{24}{C_D \cdot Re_P}\right)$$

and

$$\frac{\partial \bar{U}_P^+}{\partial y^+} = 0 \quad \text{for } y^+ = R^+. \qquad [42]$$

These boundary conditions imply that the particle concentration drops to zero at one particle radius from the wall. At the centre of the tube, symmetry conditions are employed and the particles move relative to the fluid at the settling velocity.

A discrete grid for the y direction is now devised. The first gridpoint is taken at $y^+ = d_P^+/2$, and after a very small grid spacing ($\Delta y^+ = 10^{-3}$) the grid spaces are expanded by a factor of 1.10. The grid is then given as:

$$j \leqslant 2: \begin{cases} y_1^+ = \dfrac{d_P^+}{2} \\ y_2^+ = \dfrac{d_P^+}{2} + 0.001 \end{cases}$$

$$j > 2: y_j^+ = (y_{j-1}^+ - y_{j-2}^+) \cdot 1.10 + y_{j-1}^+. \qquad [43]$$

The fields $\bar{\epsilon}$, $\bar{U}_P$ and $\bar{V}_P$ are now stored in each gridpoint. The fine grid resolution near the wall is due to the thin concentration boundary layer for Brownian diffusion. The concentration boundary layer thickness δ^+ can be estimated to be (Davies 1972):

$$\delta^+ \approx 10\,\mathrm{Sc}^{-1/3}.$$

The grid employed herein is therefore good for $\mathrm{Sc} < 10^9$ as we will then have several gridpoints within the diffusion boundary layer. For $\mathrm{Sc} > 10^9$, the particle diameter is large enough for turbulent dispersion to dominate over diffusion. Turbulent dispersion dominates over Brownian diffusion at the wall if

$$v_t^+\left(\frac{d_P^+}{2}\right) > \mathrm{Sc}^{-1}. \qquad [44]$$

From the insertion of [25] and [34] into [44] we obtain that Brownian diffusion can be neglected when

$$\mathrm{Sc} > 23.2 \cdot \mathrm{Ei}^{-2/3}. \qquad [45]$$

A typical value of Ei in air at room temperature is $\mathrm{Ei} = 10^{-7}$, with the result that Brownian diffusion is only important for $\mathrm{Sc} < 10^6$. Accordingly, the grid employed will always have several gridpoints in the Brownian diffusion boundary layer when this mechanism is of importance.

The $\overline{\epsilon^+}$ and $\overline{V_P^+}$ equations are solved by the Euler backwards differencing scheme. The $\overline{V_P^+}$ equation is solved by starting at $y^+ = R^+$ and then marching from gridpoint to gridpoint towards $y^+ = d^+/2$. The $\overline{\epsilon^+}$ equation is solved in the opposite direction, starting from $y^+ = d^+/2$ and then marching towards $y^+ = R^+$.

The $\overline{U_P^+}$ equation is solved by a standard implicit technique for elliptic partial differential equations. The actual technique employed here is the "tri-diagonal-matrix-algorithm" which is outlined in detail by Patankar (1980).

Initially the fields are given by [39] and [40] for $\overline{U_P^+}$ and $\overline{V_P^+}$. $\overline{\epsilon^+} = 1.0$ is the initial void fraction at all the gridpoints. The average bulk void fraction is now defined as

$$\epsilon_B = \frac{2}{R^{+2}} \int_{r^+=0}^{R^+} \bar{\epsilon}(y^+) r^+ \, \mathrm{d}r^+, \quad r^+ = R^+ - y^+; \qquad [46]$$

and the dimensionless average void fraction is then

$$\epsilon_B^+ = \frac{2}{R^{+2}} \int_{r^+=0}^{R^+} \bar{\epsilon}^+(y^+) r^+ \, \mathrm{d}r^+ \equiv 1. \qquad [47]$$

Assume that we have previously calculated $\epsilon_{B,P}^+$. Then the mass transfer coefficient k^+ is given by

$$k^+ = \frac{k}{u_\tau} = \frac{J}{\epsilon_{B,P} \cdot u_\tau} = \frac{J}{\epsilon_B u_\tau \left(\dfrac{\epsilon_{B,P}}{\epsilon_B}\right)} = \frac{J^+}{\epsilon_{B,P}^+}. \qquad [48]$$

At this step it is important to note that for an unconverged set of equations the previous or intermediate value of ϵ_B^+, namely $\epsilon_{B,P}^+$, may deviate considerably from 1.0 depending on the initial guess of J^+.

The equations are now solved interatively:

1. Initialize $\bar{U}_P^+$, $\bar{V}_P^+$ and $\bar{\epsilon}^+$ as described above. Set initial guess of J^+.
2. Solve for $\bar{U}_P^+$, $\bar{V}_P^+$ and ϵ^+.
3. Calculate $k^+ = J^+/\epsilon_{B,P}^+$, where $\epsilon_{B,P}^+$ is defined by [46] with ϵ replaced by ϵ^+.
4. Check if the previous value of the average bulk void fraction $\epsilon_{B,P}^+$ deviates from 1.0 by more than ± 0.01. If the deviation is greater we take $J^+ = k^+$ and return to Step 2.
5. Solution has converged. The final mass transfer coefficient is

$$k^+ = J^+$$

and [47] is fulfilled.

It was not necessary to underrelax the solutions for the fields from iteration to iteration. Convergence is established after 2–10 iterations, depending on how far the initial guess for J^+ is from its final value.

RESULTS

The theoretical results can now be tested against experimental results. The deposition data of Liu & Agarwal (1974) span over a fairly large range of t_P^+ and two different Reynolds numbers. They used urea particles deposited on a glass tube. In their experiments the shear velocities were given as $u_\tau = 0.745$ and 3.12 m/s. The carrier gas was air at room temperature, and the density ratio between aerosol particles and the gas was given as $\rho_P/\rho_F = 833$. They found that particles generated in this type of aerosol generator only carried a few electrical charges. The aerosol cloud was electrically neutral with a bipolar charge distribution. The standard deviation of charge for 1.75 μm particles from the aerosol generator was found to be 4.6e.

The experimental conditions are summarized in table 1.

The particle charge was assumed to be

$$q = 4.6\,e \cdot \left(\frac{d_P}{1.75\,\mu\text{m}}\right)^2$$

during the preliminary calculations. Figures 1–4 show how $\bar{V}_P$, $\bar{U}_P - \bar{U}_F$ and $\bar{\epsilon}$ vary through the inner velocity boundary layer for different values of t_P^+ when the physical conditions correspond to run 1 in table 1. Larger values of t_P^+ increased the pumping of particles towards the wall. The transversal lift and turbulent migration are the mechanisms responsible for this effect. Figure 4 shows the situation for $t_P^+ = 50$. Now both $\bar{V}_P$ and $\bar{U}_P - \bar{U}_F$ increase as the wall is approached. The large values of $\bar{V}_P$ close to the wall remove the particle build-up close to the walls. The simulations showed that at $t_P^+ \approx 9.95$ the situation in the boundary layer could be compared with figure 2, while $t_P^+ \approx 9.96$ caused an abrupt change in the $\bar{U}_P$ and $\bar{V}_P$ fields and the field distributions were comparable with figures 3 and 4.

The major difference in the fields below $t_P^+ \approx 9.95$ and above $t_P^+ \approx 9.96$ is found in the normal velocity $\bar{V}_P$ and the relative velocity $\bar{U}_P - \bar{U}_F$. Up to $t_P^+ \approx 9.95$ the ensemble-averaged normal to wall velocity $\bar{V}_P$ is zero and the relative velocity $\bar{U}_P - \bar{U}_F$ is small. As a consequence, the particle build-up in the boundary layer increases with increasing t_P^+ until $t_P^+ > 9.95$. From $t_P^+ \approx 9.96$ $\bar{V}_P$ takes a finite value at the wall and $\bar{U}_P - \bar{U}_F$ now takes much larger values than for $t_P^+ < 9.95$. For

Table 1. Basic data for the experiments of Liu & Agarwal (1974)

Run No.	u_τ(m/s)	R^+	ρ_P/ρ_F	$\frac{gv}{u_\tau^3}$	Ei	Mi	t_P^+
1	0.745	310	833	$3.71 \cdot 10^{-4}$	$7.42 \cdot 10^{-8}$	?	1–50
2	3.12	1300	833	$5.06 \cdot 10^{-5}$	$3.11 \cdot 10^{-7}$	?	5–200

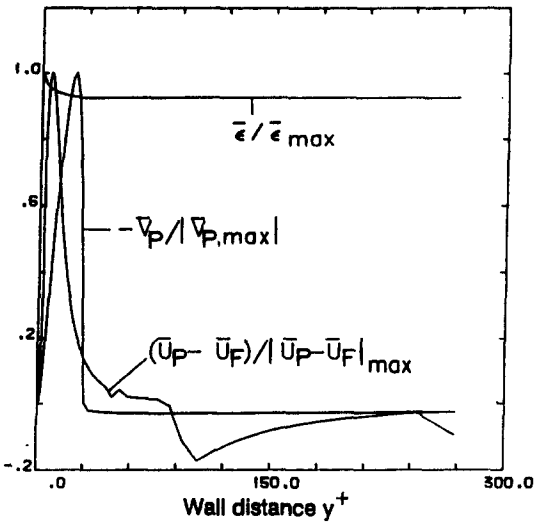

Figure 1. Predicted profiles of $\bar{\epsilon}/\bar{\epsilon}_{max}$, $(\bar{U}_P - \bar{U}_F)/|\bar{U}_P - \bar{U}_F|_{max}$ and $-\bar{\nabla}_P/|\bar{\nabla}_{P,max}|$ for $t_P^+ = 0.1$. The physical conditions are given by run 1 in table 1 and the electrostatic charging factor is $\mathscr{E} = 0.003$.

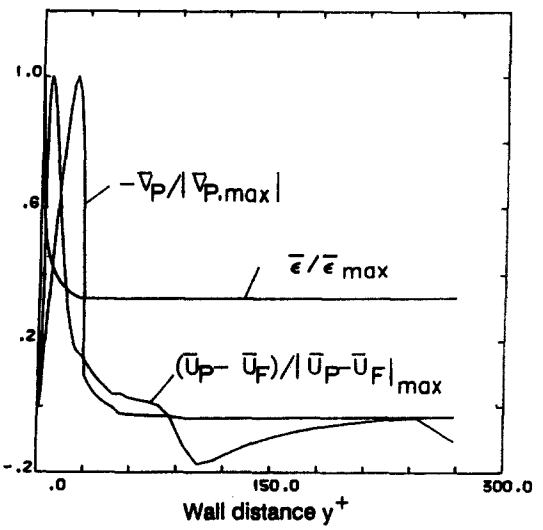

Figure 2. Predicted profiles of $\bar{\epsilon}/\bar{\epsilon}_{max}$, $(\bar{U}_P - \bar{U}_F)/|\bar{U}_P - \bar{U}_F|_{max}$ and $-\bar{\nabla}_P/|\bar{\nabla}_{P,max}|$ for $t_P^+ = 1.0$. The other physical conditions are the same as for figure 1.

increasing t_P^+ ($t_P^+ \geqslant 9.96$) the near-wall particle concentration assumes lower values while $\bar{\nabla}_P$ and $\bar{U}_P - \bar{U}_F$ increases.

The situation described above is further displayed in figure 5. The predicted profiles of $\bar{\epsilon}$ are compared for five different t_P^+. For $t_P^+ < 9.95$, $\bar{\epsilon}$ builds up in the wall region; while $t_P^+ > 9.96$ shows a situation with $\bar{\epsilon}$ in the near-wall region. For $t_P^+ = <0$, $\bar{\epsilon}$ peaks at the lower wall, but the peak is small compared with the situation for $t_P^+ < 9.95$.

When simulations were carried out for run 2 in table 1, it was found that the change in the near-wall profiles discussed above, took place for t_P^+ between 7.48 and 7.49. The major cause for this behaviour is that the value of gv/u_τ^3 is now only 14% of its value in run 1. Hence, the analyses show that there exists a critical value of t_P^+, above which resistance against deposition through the boundary layer is low. This critical t_P^+ seems to increase with increasing gv/u_τ^3.

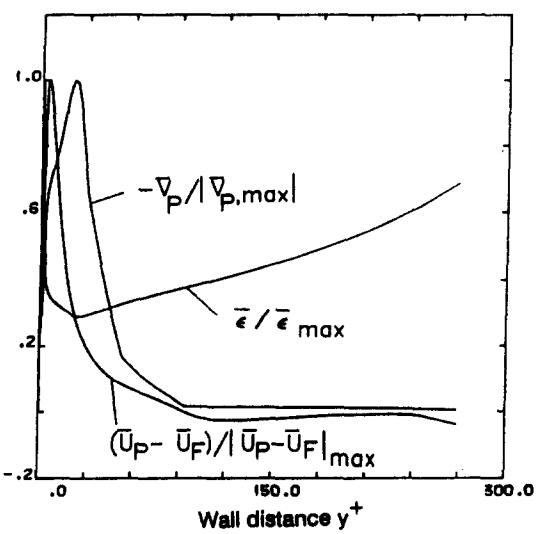

Figure 3. Predicted profiles of $\bar{\epsilon}/\bar{\epsilon}_{max}$, $(\bar{U}_P - \bar{U}_F)/|\bar{U}_P - \bar{U}_F|_{max}$ and $-\bar{\nabla}_P/|\bar{\nabla}_{P,max}|$ for $t_P^+ = 10.0$. The other physical conditions are the same as for figure 1.

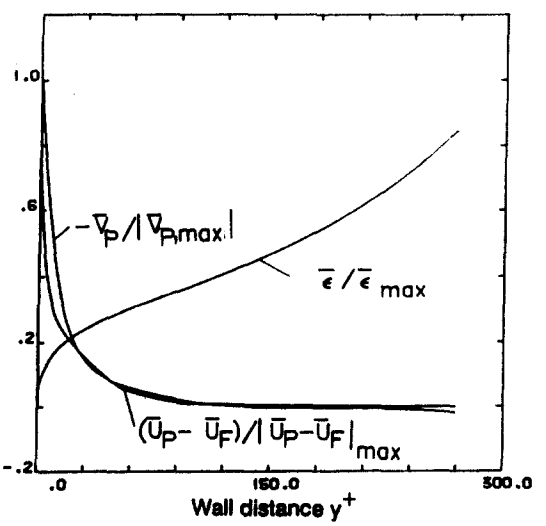

Figure 4. Predicted profiles of $\bar{\epsilon}/\bar{\epsilon}_{max}$, $(\bar{U}_P - \bar{U}_F)/|\bar{U}_P - \bar{U}_F|_{max}$ and $-\bar{\nabla}_P/|\bar{\nabla}_{P,max}|$ for $t_P^+ = 50.0$. The other physical conditions are the same as for figure 1.

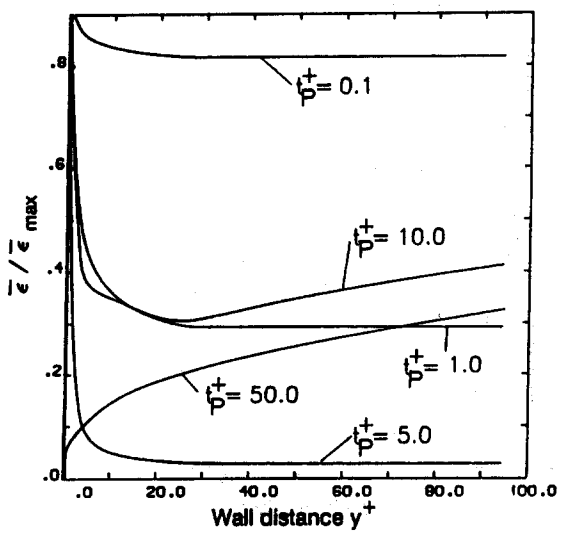

Figure 5. Comparison of predicted profiles of $\bar{\epsilon}/\bar{\epsilon}_{max}$, for different values of t_P^+. Here t_P^+ takes the values of 0.1, 1.0, 5.0, 10.0 and 50.0. The other physical conditions are the same as for figure 1.

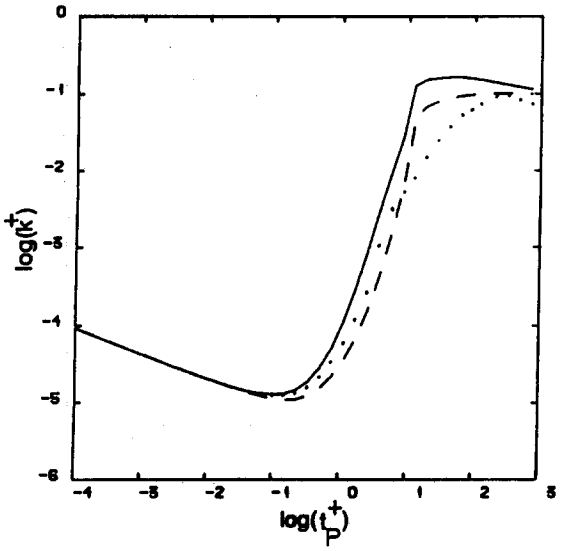

Figure 6. Predicted dimensionless mass transfer coefficient k^+ vs t_P^+ for the physical conditions given by run 1 in table 1. The electrostatic charging factor is $\mathscr{E} = 0.003$. The dotted line is obtained when the transverse lift term is omitted from [29]. The dashed line results when only the turbulent migration term is omitted and the solid line is the result when all terms are retained.

Predicted mass transfer coefficients for run 2 are given in figure 6. The figure demonstrates the influence of the turbulent migration and the transversal lift on the deposition rate. For $t_P^+ < 0.1$, the deposition is completely determined by Brownian diffusion and turbulent dispersion. In the region $1.0 < t_P^+ < 9.95$, the predicted deposition rate mainly results from the turbulent migration term; while for $t_P^+ > 9.96$, the transversal lift is the dominating effect. For $t_P^+ > 200$, the lift and the migration terms contribute equally to the deposition flux.

The maximum deposition rate close to $t_P^+ = 15$ is a result of a combination of the lift and turbulent migration mechanisms, which interact strongly in this regime ($12 < t_P^+ < 50$). For $t_P^+ > 50$, the deposition rate drops for increasing t_P^+. The physical explanation is found in the turbulent migration term, which, according to [35], creates a drift away from the wall for $y^+ > 30$. For large t_P^+, there is no resistance against deposition in the inner boundary layer, and the deposition is governed by the turbulent migration and dispersion in the bulk flow. From [17], [35] and [40] it is expected that increasing t_P^+ will result in a reduced deposition rate until $t_P^+ \gg \tau_L^+$ throughout the bulk fluid.

The electrostatic forces due to mirror charging are now investigated. The maximum charging of a particle is, according to Hesketh (1977):

$$q_{max} = 500\, e \left(\frac{d_P}{10^{-6}\,\mathrm{m}}\right)^2; \quad d_P > 10^{-7}\,\mathrm{m}. \qquad [49]$$

The particle charge is therefore assumed to be a given fraction $\mathscr{E}$ of the maximum charge q_{max}, which gives

$$q = \mathscr{E} \cdot q_{max}; \quad \mathscr{E} \leqslant 1.0. \qquad [50]$$

Calculated deposition rates for $\mathscr{E} = 0.0$, 0.1 and 1.0 are shown in figure 7. The deposition rate is strongly enhanced by electrical charges for intermediate t_P^+. This surprisingly strong effect is caused by the turbulent migration which pumps particles into the wall boundary layer. The electrostatic forces are of short range, but extremely close to the wall they dominate over Brownian diffusion and turbulent dispersion. Hence, the near-wall resistance against deposition is lowered by increased particle charge and the deposition rate will increase.

The theoretical deposition rates can now be compared with the experiments of Liu & Agarwal (1974). We first consider the situation given in table 1, run 1. The electrical particle charge

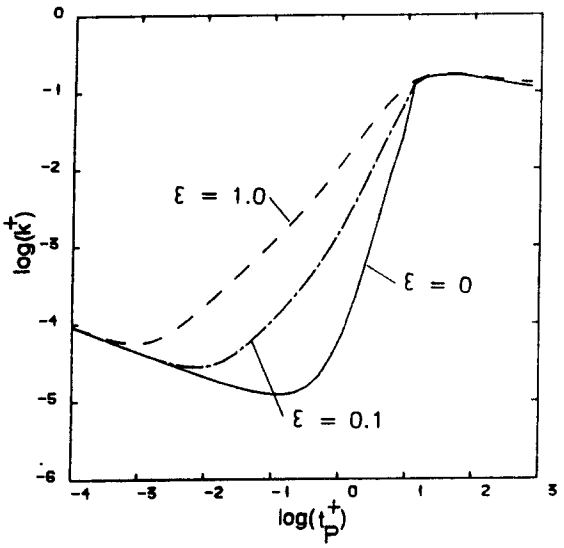

Figure 7. Influence of electrostatic charge on the deposition rate k^+ vs t_P^+. The fraction of particle electrostatic charge to the maximum charge is $\mathscr{E}$, which takes the values $\mathscr{E} = 0.0$, 0.1 and 1.0. The physical conditions are given by run 1 in table 1.

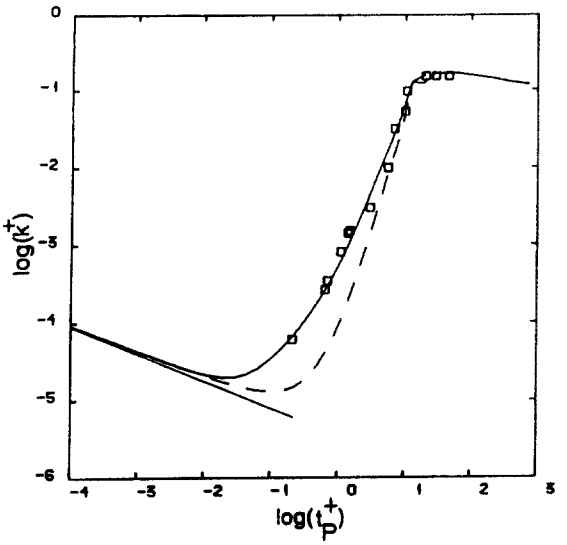

Figure 8. Comparison of predicted deposition mass transfer coefficients k^+ with the experimental data of Liu & Agarwal (1974) (□) and the mass transfer data of Campbell & Hanratty (1983) (——, lowest straight line). The experimental situation is given in run 1 in table 1. The dashed line represents the charging factor $\mathscr{E} = 0.003$ reported from one experiment (Liu & Agarwal 1974), while the solid line represents $\mathscr{E} = 0.03$.

reported by Liu & Agarwal corresponds to $\mathscr{E} = 0.003$ in [50]. However, they measured the charge distribution at the exit of their aerosol generator and it is reasonable to expect that the decharged particles might pick up a few more charges on their way from the aerosol generator to the test section. We have therefore taken $\mathscr{E} = 0.03$ as a possible value for the particles in the test section.

The result is seen in figure 8. The value of $\mathscr{E} = 0.003$, given by the experiments of Liu & Agarwal (1974), lead to an underprediction of the deposition rate for $t_P^+ \leqslant 2$. However, the suggested value of $\mathscr{E} = 0.03$ gives excellent agreement between the theoretical predictions and the experiments. For $t_P^+ \leqslant 0.1$ the deposition is mainly governed by Brownian diffusion. In this region our results are compared with the experimental data of Campbell & Hanratty (1983). They found that the mass transfer rate k^+ for large Sc is

$$k^+ = 0.09 \cdot \mathrm{Sc}^{-0.7}. \qquad [51]$$

With the help of [25] and [38] the mass transfer rate is rewritten as

$$k^+ = 0.09 \left(\mathrm{Ei} \frac{\rho_P}{18 \rho_F t_P^+} \right)^{0.7}. \qquad [52]$$

From figure 8 it can be seen that the experimental results, given by [52], are very well reproduced by the present theory.

Similarly, the theoretical predictions for run 2 in table 1, are compared with experiments in figure 9. The experimental data show slightly larger deposition rates than the predictions for the lowest data point. However, in general, the agreement between predictions and experiments is excellent. Also, in the Brownian deposition regime the predictions fit the experimental data represented by [52] satisfactorily.

It is interesting to note that the tube Reynolds number has an influence on the deposition rate. Both the experiments and the predictions give a maximum deposition rate which is largest for the smallest Reynolds number (run 1). The Reynolds number effect is clearly shown in figure 10, where the predicted deposition rates for $t_P^+ = 20$ decay with increasing tube Reynolds number $R^+ = Ru_\tau/\nu$.

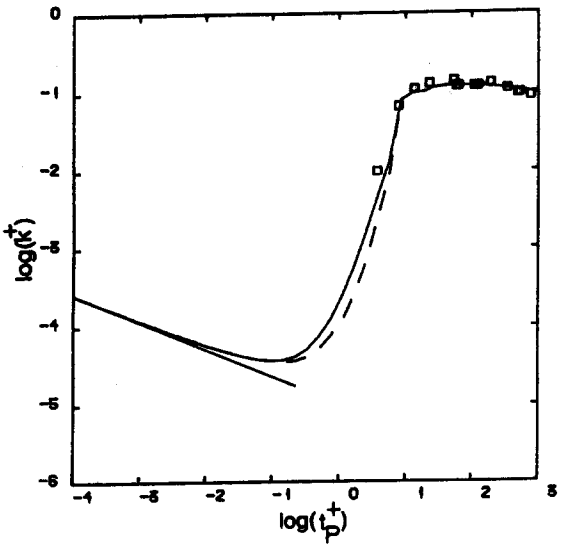

Figure 9. Comparison of predicted deposition mass transfer coefficients k^+ with the experimental data of Liu & Agarwal (1974) (□) and the mass transfer data of Campbell & Hanratty (1983) (——, lowest straight line). The experimental situation is given by run 2 in table 1. The dashed line represents the charging factor $\mathscr{E} = 0.003$ reported from one experiment (Liu & Agarwal 1974), while the solid line represents $\mathscr{E} = 0.03$.

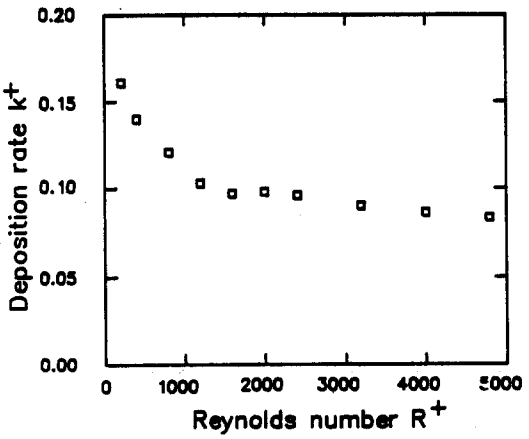

Figure 10. Predicted deposition mass transfer coefficients k^+ vs the tube Reynolds number $R^+ = R \cdot u_\tau/\nu$. The data corresponds to run 1 in table 1, and only the tube radius R is varied in order to achieve different values of R^+.

In these simulations the gravity group $(g\nu/u^3)$ has been kept constant, and except for R^+ the input data was as for run 1, table 1.

It is now interesting to see the effects of the flow direction. So far we have considered a downward flow where the lift force always cause a migration towards the wall. The flow direction is easily reversed by changing the sign of the gravitational acceleration. It was quite surprising to find that the predicted deposition rates for an upward flow are surprisingly similar to the predictions shown in figures 8 and 9. It was expected that the particle velocity would be less than the fluid velocity, due to settling in an upward flow. However, the turbulent migration mechanism creates a drift of particles through the boundary layer from regions with large $\bar{U}_F$ to regions with smaller fluid

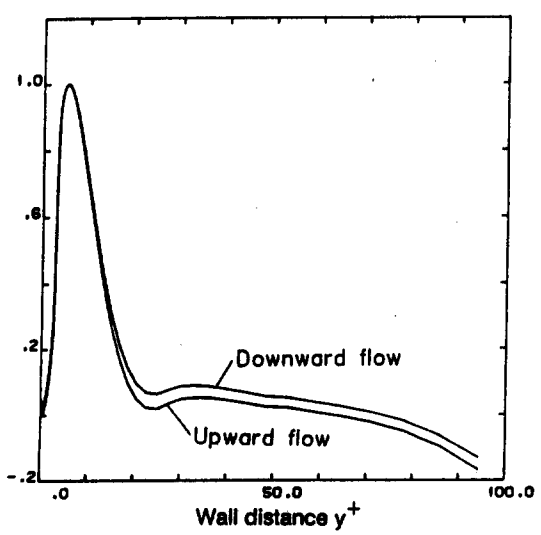

Figure 11. Comparison of normalized axial relative velocities $(\bar{U}_P - \bar{U}_F)/|\bar{U}_P - \bar{U}_F|_{max}$ for downward and upward vertical flows. The physical conditions are given by run 1 in table 1; $t_P^+ = 5.0$ and $\mathscr{E} = 0.003$.

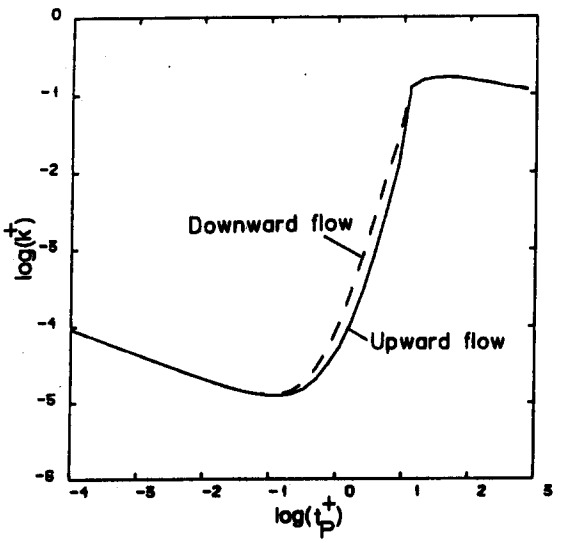

Figure 12. Predicted influence of transport direction (upwards or downwards) on the deposition rate k^+ for run 1 in table 1 and $\mathscr{E} = 0.003$.

velocities. The particles can therefore obtain larger U velocities than the fluid if they move fast enough in the direction of smaller $\bar{U}_F$. When the particle inertia increases, the particles will retain more and more of their axial bulk velocity on their way through the boundary layer. Also, turbulent dispersion plays an active role in equalizing the axial particle velocity. Turbulent dispersion will therefore speed up the axial particle velocity in the inner boundary layer and reduce the axial velocity in the bulk flow. The result of both mechanisms in combination is that the particle velocity can be lower than the fluid velocity in the core of the flow and larger than the fluid velocity in the wall boundary layer, regardless of flow direction. Such behaviour is demonstrated in figure 11. This result is restricted to a situation where particles deposit on the wall, and there are actual situations where settling will dominate over drift and dispersion in the bulk flow.

In figure 12 the theoretical deposition rates are compared for upward and downward flow. For $0.1 < t_P^+ < 10$, it is seen that the deposition rate may be increased by a factor of 2 if the flow direction is turned from upwards to downwards. The charging coefficient was set to its lowest value ($\mathscr{E} = 0.003$) in this calculation. For small ($t_P^+ < 0.1$) and large ($t_P^+ > 10$) values of t_P^+ the deposition rate is governed by Brownian diffusion or turbulent dispersion and migration in the bulk fluid. As expected, the deposition rate is independent of the flow direction in these two regimes.

An investigation of the effects related to the gravity group gv/u_τ^3 is shown in figure 13. The calculated situation is represented by run 1, table 1. The particle charge is given by [50] and $\mathscr{E} = 0.003$. The flow direction is downwards. From figure 13 it is seen that the group variations of the shear velocity u_τ and, accordingly, the gravity group (gv/u_τ^3) result in a large range of deposition rates for a fixed value of t_P^+. This is a result of the enhanced lift forces created by larger settling velocities.

DISCUSSION

The model presented seems to represent experimental data for deposition very well, though there is room for further development of the model. The flow has been assumed to be one-dimensional and it is not possible to obtain a correct particle concentration distribution close to the centre axis as $\partial\epsilon/\partial x \neq 0$.

The boundary condition for particle momentum in the x-direction is somewhat problematic. The assumption that $J^+\bar{U}_P^+ - \bar{\epsilon}^+ v_P^+ (\partial \bar{U}_P^+ / \partial y^+) = 0$ at both boundaries implies that we have a mirror condition. A mirror wall boundary condition is achieved in practice when the particle collisions with the wall are completely elastic and no U-momentum is lost in the collisions. When the wall absorbs the particles, the situation becomes more complicated. However, there will be no transport of U-momentum from the wall to the laminar sublayer and the positive flux from the wall to the first near-wall node must be zero. In general, it is preferred to have wall functions which can link the near-wall concentration to the wall shear stress imposed by the particles. At the symmetry line the mirror boundary condition is not a problem.

The analyses presented herein shows that the particle deposition process can be accurately analysed by Reynolds-averaged Eulerian transport equations based on standard gas–particle interaction theories available from the literature. The results indicate that electrical charges may play an important role in the deposition process for t_P^+ between 0.1 and 10.0. However, it is still a possibility that there are other physical mechanisms, not considered herein, which can explain the experimental data with the reported charge distribution. For example, can thermophoresis play an important role if temperature gradients are present? Work being carried out presently by the author seems to indicate that if the wall temperature was just a few degrees (2–4 K) below the bulk of the gas this would be sufficient to explain the experimental deposition rates even without the mirror charging effect.

A full validation of these mechanisms is not possible since exact temperatures as well as the particle charge distribution at the entrance of the test section were not measured in the experiments of Liu & Agarwal (1974). However, the Liu & Agarwal data are, to the best of the author's knowledge, hitherto by far the best data available in the literature.

Further, the present analysis offers some explanations of the large scatter in the experimental data reported in the literature (Papavergos & Hedley 1984). Davies (1983) argues that the deposition data can be represented by a description of dimensionless surface roughness height

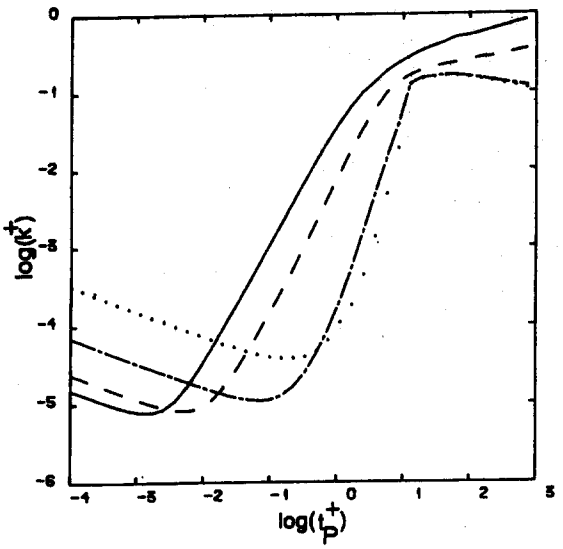

Figure 13. Investigation of the importance of the gravity group (gv/u_τ^3) by varying the shear velocity u_τ for otherwise equal conditions, as given by run 1 in table 1 and $\delta = 0.003$; ——, $u_\tau = 0.05$, $(gv/u_\tau^3) = 1.23$; – – – –, $u_\tau = 0.1$, $(gv/u_\tau^3) = 1.54 \cdot 10^{-1}$; —·—·—, $u_\tau = 0.5$, $(gv/u_\tau^3) = 1.23 \cdot 10^{-3}$; · · · · · ·, $u_\tau = 5.0$, $(gv/u_\tau^3) = 9.83 \cdot 10^{-6}$.

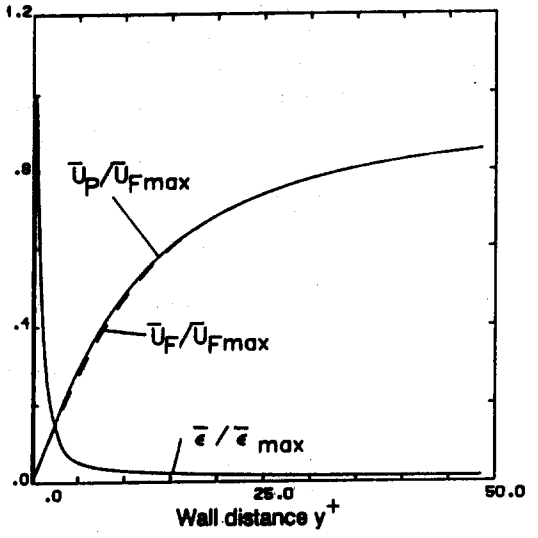

Figure 14. Predicted profiles of $\bar{\epsilon}/\bar{\epsilon}_{max}$, $\bar{U}_P/\bar{U}_{F,max}$ and $\bar{U}_F/\bar{U}_{F,max}$ for zero mass transfer $(|J^+| \equiv k^+ \equiv 0)$ for the situation analysed in figure 15.

distributions and the particle relaxation time t_P^+. Indeed, the surface roughness is an important quantity which has been omitted in the present analysis. However, the present results for downward transport given in figure 13 show that the gravity group (gv/u_τ^3) is an extremely important factor. For $t_P^+ \approx 1$, the deposition rate is seen to vary by almost 3 orders of magnitude if (gv/u_τ^3) is varied by the same amount. According to Papavergos & Hedley (1984), the experimental data range between $k^+ \approx 10^{-5}$ and 10^{-2} for $t_P^+ = 1.0$. This compares favourably with the calculated values which range from $k^+ = 10^{-4}$ to $5 \cdot 10^{-2}$ (see figure 13). The effect of surface roughness in the deposition process will be easier to analyse in the future if the effects related to the gravity group (gv/u_τ^3) are accounted for.

The physical interpretation of the gravity group for downward transport is that, for small u_τ and larger values of (gv/u_τ^3), the deposition process is governed more and more by the lift forces. This is explained by the reduction in u_τ, while $t_P^+ = \text{const}$, which corresponds to an increasing particle diameter and, accordingly, larger relative velocities. At small values of (gv/u_τ^3) and large u_τ $(u_\tau > 0.5)$, the deposition rate is only slightly dependent on (gv/u_τ^3). The explanation here is that for large u_τ, the axial interphasial relative velocities are dominated by the transverse particle movement in the boundary layer and not by gravitational setling.

For upward transport an increased value of (gv/u_τ^3) will most likely lead to larger relative velocities in the bulk flow but reduced relative velocities in the boundary layer. Upon further increasing the gravity group, the near-wall particles are expected to lag behind the fluid in the boundary layer or even move in the countercurrent direction. If the average fluid velocity becomes smaller than $u_\tau t_P^+ (gv/u_\tau^3)$, the particles can not be transported upwards as their settling velocity becomes larger than the fluid velocity. Anyway, it should be obvious that the gravity group, if increased in upward transport, will lead to a reduced deposition rate.

The Reynolds number, here represented by $R^+ = Ru_\tau/v$, is alone responsible for variations in the dimensionless deposition rate k^+. In figure 10 it was shown that the Reynolds number can at least alter k^+ by a factor of 2. The larger deposition rate in the data of Liu & Agarwal (1974) for the lowest R^+ (run 1, table 1) is explained as a pure Reynolds number effect. From the results shown in figure 13 it is not expected that variations in the gravity group would influence the experimental deposition data for $t_P^+ > 10$ as $(gv/u_\tau^3) \ll 1.23 \cdot 10^{-3}$ in the experiments.

The explanation for the Reynolds number effect is that for a low $\text{Re} = R\bar{U}_{max}/v$ and, accordingly, a small R^+, the wall layer where turbulent migration and the lift mechanism dominate contains

a relatively larger fraction of the fluid. Hence, the concentration gradients in the bulk fluid become steeper and the turbulent transport in the bulk will be more effective.

Another interesting result is that the employed eddy viscosity distribution represented by [34] and the turbulent Schmidt number ([15]) give a very good prediction of Brownian diffusion (see figures 8 and 9). The predicted Schmidt number dependence for the mass transfer rate for very small t_P^+ is close to the experimental data which give $k^+ \sim Sc^{-0.7}$. Increasing t_P^+ gives increasing particle diameter for constant u_τ and, hence, the boundary condition $\epsilon^+(d_P^+/2) = 0$ will result in a larger deposition rate for particles than for a diffusing chemical species.

The importance of the lift forces and the turbulent migration mechanism should make it possible to obtain larger deposition rates in entrance regions where the flow is undeveloped and the gradients in the flow fields are large.

The model has several other very interesting implications. The model offers an explanation for a question which has occupied researchers for many years, namely the possibility of the particles having a larger diffusivity than the fluid. Goldschmit *et al.* (1972) showed that the particles can have a larger diffusivity than the fluid in turbulent jets. This result contradicts the classical theories (Pourahmadi 1982; Gouesbet *et al.* 1984; Picart *et al.* 1986; Desjonquers *et al.* 1986) for particle dispersion, which state that the particle diffusivity can never exceed the fluid diffusivity for any significant period of long time.

The turbulent migration mechanism, caused by gradients in the turbulent r.m.s. velocities, will create an additional dispersion of particles. This effect will, due to [17] and [40], disappear if $t_P \ll \tau_L$ or $t_P \gg \tau_L$. It is therefore reasonable that turbulent migration might affect the radial dispersion of particles in a turbulent jet where there are gradients in the radial turbulent r.m.s. velocity.

Another interesting result of the migration mechanism is the enrichment of particles in the wall boundary layer for intermediate t_P^+. Due to Pourahmadi (1982) and Elghobashi & Abou-Arab (1983), a large concentration of small particles in the wall boundary layer will lead to enhanced dissipation of the fluid turbulent energy. Then the "laminar" wall layer will increase in thickness and the wall shear stress will decrease. This effect is known as "the drag reduction" caused by small particles or macromolecules. Pourahmadi's (1982) analysis shows that dissipation due to particle–fluid interaction is proportional to $\bar{\epsilon}/(t_P + \tau_L)$ and it is therefore expected that small particles ($t_P \lesssim \tau_L$) will contribute the most to this additional dissipation. However, the present analysis shows that particles with intermediate t_P^+ build up in the boundary layer. Then a given, intermediate, particle size (not the smallest), can result in the maximum drag reduction. Figure 14 shows that a nonabsorbing wall for $t_P^+ = 10$ will give a very large near-wall particle concentration compared with an absorbing wall (figure 15). The maximum concentration for no deposition (figure 14) is 32 times the average concentration.

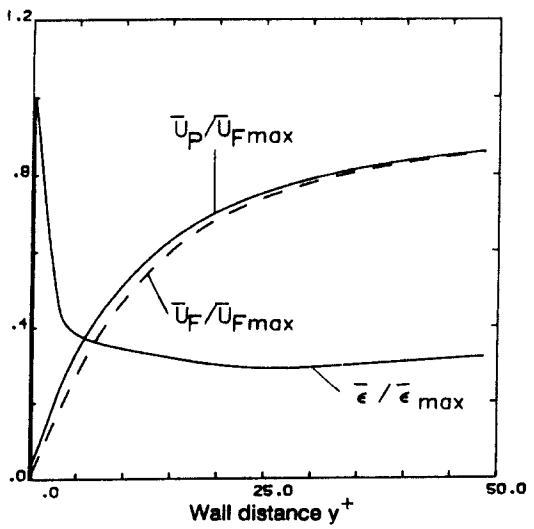

Figure 15. Predicted profiles for $\bar{\epsilon}/\bar{\epsilon}_{max}$, $\bar{U}_P/\bar{U}_{F,max}$ and $\bar{U}_F/\bar{U}_{F,max}$ for the situation given in run 1 in table 1, $\delta = 0.003$ and $t_P^+ = 10.0$ (Note that both the fluid and particle velocity are normalized with the maximum fluid velocity.) The solid line represents the particle velocity.

Another interesting result from the model is the predicted axial velocity profiles for the particle phase. The axial particle velocity component close to the wall exceeds the gas velocity due to drift and dispersion, and this effect is of major importance in explaining the observed high deposition rates in upward directed flows. Figure 16a shows the axial velocity component for the two phases in an upward directed flow. Close to the symmetry line ($y^+ = 465$) the particles lag behind the fluid at a velocity which is slightly larger than the settling velocity (shown by the arrow). Close to the wall the particle velocity exceeds the fluid velocity. This result can be compared with the experimental results of Lee & Durst (1982), given in figure 16b. The agreement is acceptable, although the point at which there is equal gas and particle velocity is $\Delta y^+ \approx 50$ in the predictions while it is roughly 50% higher ($\Delta y^+ \approx 78$) in the experiments. The momentum exchange from particles to fluid is neglected in our calculation. Therefore the particles can not accelerate the near-wall fluid, as seen in the experiments.

If the relative velocity between the phases becomes so large that particles close to the wall start to lag behind the fluid or even flow in the downward direction, the lift force will act outwards from the wall and can produce a particle-free layer close to the wall. This effect was observed by Lee & Durst (1982). We believe that these findings can be developed and may shed light on questions concerning minimum transport velocities in vertical pneumatic transport.

The physics outlined above can be of major importance in understanding particle precipitators like, for example, cyclones. The lift and turbulent migration mechanisms will contribute strongly to wall deposition and particle enrichment in the boundary layer. Large particle concentration favours agglomeration and reduces the possibility for near-wall particles to diffuse away from the wall and against the centrifugal field. However, the bi-directional coupling between the phases becomes of major importance in cyclone boundary layers, and should therefore be included in such an analysis.

The model should in the future be developed to include full coupling between the two phases. Full coupling is expected to show that the deposition process will be altered if the particle volume fraction becomes comparable with or larger than ρ_F/ρ_P.

By including mechanisms such as virtual mass, pressure terms and the Basset history force into the particle momentum equations, it is believed that the present model will yield interesting results for the deposition of particles in liquids.

The present model is now being refined to account for particle deposition by thermophoresis. To date, theoretical models for thermophoresis have not been able to reproduce the unexpectedly

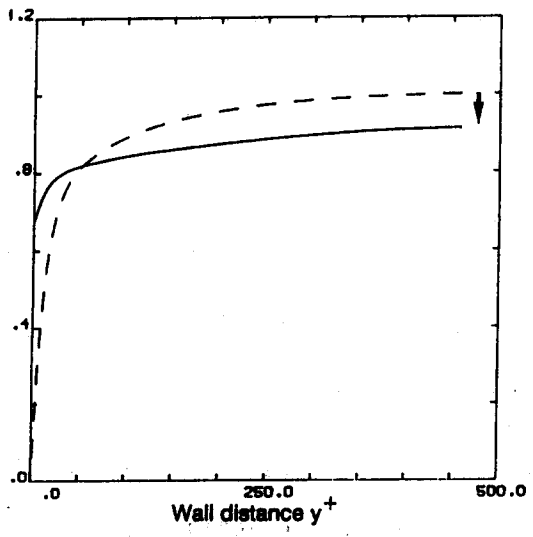

Figure 16a. Predicted particle velocity ($U_P/U_{F,max}$, ——) and the given, empirical gas velocity profile ($U_F/U_{F,max}$, – – – –) for the situation investigated experimentally by Lee & Durst (1982) for a vertical upward flow, see figure 16b. The wall is not allowed to absorb particles ($|J^+| \equiv k^+ \equiv 0$).

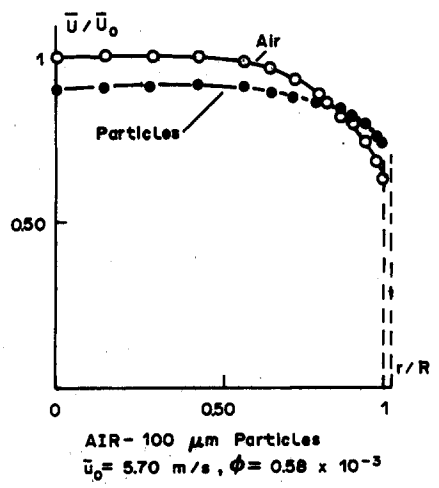

Figure 16b. Experimental data from Lee & Durst (1982) for 100 μm dia glass particles in air, tube dia = 41.8 mm and maximum gas velocity $U_0 = 5.70$ m/s. The volume fraction of particles is $0.58 \cdot 10^{-3}$ and the flow is directed vertically upwards.

high experimental deposition rates found in the literature (Johansen & Anderson 1986). This discrepancy can probably be explained by turbulent drift and an increased importance of lift forces when particles travel quickly towards the wall and carry along some of the large U-momentum from the outer boundary layer. Hence, the increased near-wall relative velocity will enhance lift forces and deposition. As the present paper indicates, electrostatic forces might be important in several deposition situations and this could well be a contributing factor in thermophoretic deposition.

CONCLUSION

The presented model for particle deposition from vertical flows shows that experimental data on particle deposition can be explained by a turbulent migration mechanism, transversal lift forces and a minor electric charge on the particles. The model can represent the data for all values of t_P^+. However, in order to achieve perfect agreement with the data in the interval $0.1 < t_P^+ < 10$, it has been assumed that the electrical charge on the particles has increased by a factor of 10 on their way from the aerosol generator to the test section.

It is shown that the deposition rate is governed by the dimensionless groups t_P^+, Mi, Ei, gv/u_τ^3 and the Reynolds number $R^+ = Ru_\tau/v$. It is therefore concluded that turbulent deposition data as function of solely t_P^+ is an inadequate representation.

The influence of surface roughness on the deposition process has not been investigated.

The physics represented by the model can explain or give ideas about several two-phase flow phenomena which have occupied researchers during the last two or three decades.

Acknowledgements—The author wishes to thank the Royal Norwegian Council for Scientific and Industrial Research for their financial support (under Project MB 63-20034).

Mrs I.G. Page is acknowledged for her patience in typing this manuscript, and Dr N.M. Anderson for correcting the English.

REFERENCES

BEAL, S. K. 1970 Deposition of particles in turbulent flow on channel or pipe walls. *Nucl. Sci. Engng* **40,** 1–11.

BESNARD, P. C. & HARLOW, F. H. 1988 Turbulence in multiphase flow. *Int. J. Multiphase Flow* **14,** 679–699.

BOOTHROYD, R. G. 1971 *Flowing Gas–Solids Suspensions*, p. 215. Chapman & Hall, London.

CAMPBELL, J. A. & HANRATTY, T. J. 1983 Turbulent velocity fluctuations that control mass transfer to a solid boundary. *AlChE Jl* **29,** 215–221.

CLEAVER, J. W. & YATES, B. 1975 A sublayer model for the deposition of particles from a turbulent flow. *Chem. Engng Sci.* **30,** 983–992.

DAVIES, C. N. 1966 *Aerosol Science*, p. 393. Academic Press, London.

DAVIES, J. T. 1972 *Turbulence Phenomena*. Academic Press, New York.

DAVIES, J. T. 1983 A new theory of aerosol deposition from turbulent flows. *Chem. Engng Sci.* **38,** 135–139.

DESJONQUERS, P., GOUESBET, G., BERLEMONT, A. & PICART, A. 1986 Dispersion of discrete particles by continuous turbulent motions: new results and discussions. *Phys. Fluids* **29,** 2147–2151.

ELGHOBASHI, S. E. & ABOU-ARAB, T. W. 1983 A two-equation turbulence model for two-phase flows. *Phys. Fluids* **26,** 931–938.

FORTIER, A. 1967 *Mecaniqe des Suspensions*. Masson & Cie, Paris.

FRIEDLANDER, S. K. & JOHNSTONE, H. F. 1957 Deposition of suspended particles from turbulent gas streams. *Ind. Engng Chem.* **49,** 1151–1156.

GOLDSCHMIT, V. W., HOUSEHOLDER, M. K., AHMADI, G. & CHUANG, S. C. 1972 Turbulent diffusion of small particles suspended in turbulent jets. *Prog. Heat Mass Transfer* **6,** 487–508.

GOUESBET, G., BERLEMONT, A. & PICART, A. 1984 Dispersion of discrete particles by continuous turbulent motions. Extensive discussions of Tchen's theory, using a two-parameter family of Lagrangian correlation functions. *Phys. Fluids* **27,** 827–837.

HESKETH, H. E. 1977 *Fine Particles in Gaseous Media*, pp. 74–89. Ann Arbor Science, Ann Arbor, Mich.

HJELMFELT, A. T. & MOCROS, L. F. 1966 Motion of discrete particles in a turbulent fluid. *Appl. scient. Res.* **16**, 149–161.

HUTCHINSON, P. & HEWITT, G. F. 1971 Deposition of solid dispersions from turbulent gas streams: a stochastic model. *Chem. Engng Sci.* **26**, 419–439.

JOHANSEN, S. T. & ANDERSON, N. M. 1986 A model for predicting effects of thermophoresis on collection efficiency in swirling flow precipitators. In *Gas Cleaning at High Temperatures. IChemE Symposium Series No. 99*, pp. 73–88. Pergamon Press, Oxford.

JOHANSEN, S. T. & YTREHUS, T. 1988 Improved wall functions for momentum, heat and mass transfer. Unpublished research.

KIM, J., MOIN, P. & MOSER, R. 1987 Turbulence statistics in a fully developed channel flow at low Reynolds number. *J. Fluid Mech.* **177**, 133–166.

KNEEN, T. & STRAUSS, W. 1969 Deposition of dust from turbulent air streams. *Atmos. Envir.* **3**, 55–67.

KUTADELADZE, S. S., KHABAKHPASHEVA, W. M., ORLOV, V. V., PEREPELITSA, P. V. & MICHAILOVA, E. S. 1979 In *Turbulent Shear Flows I*, pp. 91–103. Springer-Verlag, Berlin.

LAUNDER, B. E. 1978 *Turbulence. Topics in Applied Physics*, Vol. 12, pp. 232–284. Springer-Verlag, Berlin, 232–284.

LEE, S. L. & DURST, F. 1982 On the motion of particles in turbulent duct flows. *Int. J. Multiphase Flow* **8**, 125–146.

LIU, B. Y. H. & AGARWAL, J. K. 1974 Experimental observation of aerosol deposition in turbulent flow. *J. Aerosol Sci.* **5**, 145–155.

LIU, B. Y. H. & ILORI, T. Y. 1974 Aerosol deposition in turbulent pipe flow. *Envir. Sci. Technol.* **8**, 351–356.

MATTESON, J. M., SANDLIN, C. W. & PREINING, O. 1973 Diffusion of aerosols at various temperatures. *Aerosol Sci.* **4**, 307–315.

MAXEY, M. R. & RILEY, J. J. 1983 Equation of motion for a small rigid sphere in a nonuniform flow. *Phys. Fluids* **26**, 883–889.

MEDNIKOW, E. P. 1985 Theory of movement of sediment. *Met. Gidrol.* **82**, 68–79.

MORSI, S. A. & ALEXANDER, A. J. 1972 An investigation of particle trajectories in two-phase systems. *J. Fluid Mech.* **55**, 193–208.

NIGMATULIN, R. I. 1979 Spatial averaging in the mechanics of heterogeneous and dispersed system. *Int. J. Multiphase Flow* **5**, 353–385.

OWEN, P. R. 1960 *Aerodynamic Capture of Particles*, p. 8. Pergamon Press, Oxford.

PAPAVERGOS, P. G. & HEDLEY, A. B. 1979 Particle deposition behaviour in fully developed turbulent flows. In *Multiphase Transport*, Vol. 4 (Edited by VEZIROGLU, T.N.), pp. 1893–1921. Hemisphere, Washington, D.C.

PAPAVERGOS, P. G. & HEDLEY, A. B. 1984 Particle deposition from turbulent flows. *Chem. Engng Res. Dev.* **62**, 275–295.

PATANKAR, S. V. 1980 *Numerical Heat Transfer and Fluid Flow*. Hemisphere, Washington, D.C.

PICART, A., BERLEMONT, A. & GOUESBET, B. 1986 Modelling and predicting turbulence fields and the dispersion of discrete particles transported by turbulent flows. *Int. J. Multiphase Flow* **12**, 237–261.

POURAHMADI, F. 1982 Turbulence modeling of single and two phase curved channel flows. Ph.D. Thesis, Univ. of California, Berkeley.

REEKS, M. W. 1983 The transport of discrete particles in inhomogeneous turbulence. *J. Aerosol Sci.* **14**, 729–739.

REEKS, M. W. & SKYRME, G. 1976 The dependance of particle deposition velocity on particle inertia in turbulent pipe flow. *J. Aerosol Sci.* **7**, 485–495.

REYNOLDS, A. J. 1975 The prediction of turbulent Prandtl and Schmidt numbers. *Int. J. Heat Mass Transfer* **18**, 1055–1069.

ROGERS, M. M., MOIN, P. & REYNOLDS, W. C. 1986 The structure and modelling of the hydrodynamic and passive scalar fields in homogeneous turbulent shear flow. Report TF-15, Dept Mech. Engng, Stanford Univ., Calif.

ROUHIAINEN, P. O. & STACHIEWICZ, J. W. 1970 On the deposition of small particles from turbulent flows. *J Heat Transfer* **92,** 169–177.

SAFFMAN, P. G. 1965 The lift on a small sphere in a slow shear flow, *J. Fluid Mech.* **22,** 385–400. Corrigendum (1968) *J. Fluid Mech.* **31,** 624.

TALBOT, L., CHENG, R. K., SCHEFER, R. W. & WILLIS, D. R. 1980 Thermophoresis of particles in a heated boundary layer. *J. Fluid Mech.* **101,** 737–758.

TENNEKES, H. & LUMLEY, J. L. 1972 *A First Course in Turbulence.* MIT Press, London.